Effects of temperature and pressure on the stability and mobility of phases in rigid rod poly (*p*-phenylenes)

A. Gitsas and G. Floudas*
Department of Physics, University of Ioannina, P.O. Box 1186, 451 10 Ioannina, Greece
and Foundation for Research and Technology–Hellas (FO.R.T.H), Biomedical Research Institute (BRI), Ioannina, Greece

G. Wegner
Max-Planck Institut für Polymerforschung, Postfach 3148, D-55021 Mainz, Germany
(Received 16 October 2003; published 30 April 2004)

The structure and the associated dynamics have been investigated in melts of hairy-rod macromolecules composed from a poly(*p*-phenylene) backbone with sulfonate ester and dodecyl side chains. For the structure investigation, polarizing optical microscopy, differential scanning calorimetry, pressure-volume-temperature, and wide-angle x-ray scattering have been employed whereas for the dynamics dielectric spectroscopy as a function of temperature and pressure was used. Based on the combined information from structure and dynamics the relaxation mechanisms were identified and the origin of the glass transition has been discussed in terms of insufficient thermal energy rather than insufficient free volume. The relevant phase diagram has been constructed and the stability and mobility of phases is discussed.

DOI: 10.1103/PhysRevE.69.041802 PACS number(s): 36.20.−r, 64.70.Md, 61.41.+e, 77.84.Nh

I. INTRODUCTION

Hairy-rod macromolecules belong to a class of materials known as ''shape persistent'' molecules with possible applications as elements of construction for larger scale molecular devices (for a recent review see [1]). These materials are envisioned as molecular rods embedded in a continuous matrix of the liquidlike side chains and, in this respect, they can be considered as ''molecular composites.'' The polymer backbone is composed mainly from poly(*p*-phenylene) (PPP) that provides the required stiffness and flexible side chains are attached to the backbone to improve solubility and avoid aggregation. The system under investigation consists of a poly(*p*-phenylene) backbone with sulfonate ester and dodecyl side chains. The dodecyl chains alternate with the voluminous sulfonate ester groups as side chains and it is this property that provides the good solubility of the polymer in conventional solvents [2].

The present investigation is a part of an ongoing effort in exploring the complex dynamics in systems possessing intrinsic orientational order. Recently we identified the molecular origin of the dynamic processes in rigid-rod poly (*p*-phenylenes) with short ethylene oxide (EO) side chains using dielectric spectroscopy and NMR [3]. Two processes were identified, called α and β, with distinctly different temperature and pressure dependencies. The β process with a low activation energy and low activation volume reflected a very localized motion of the outer ethylene oxide side chains, whereas the slower α process associated with the glass transition. The molecular origin of the α process was complex comprising at lower temperatures the outer EO units, at intermediate temperatures small-angle fluctuations of the substituted rings, and at higher temperatures, the unfreezing of the backbone dynamics, including bending modes.

The dynamics in substituted poly(*p*-phenylenes) with sulfonate ester and dodecyl side chains have been studied [4] in toluene solutions up to 50% in concentration with depolarized light scattering and dielectric spectroscopy probing, respectively, the backbone and polar side group orientational dynamics. The main findings were (i) the presence of a non-Debye orientational relaxation for dilute solutions ($c=4\%$) in the isotropic state, and (ii) the coupling of the main-chain dynamics with the side-chain dynamics for concentrations above 50%.

In the present investigation we study the structure and the associated dynamics of the same poly(*p*-phenylenes) with sulfonate ester and dodecyl side chains in the absence of solvent. For the structure investigation we employed, polarizing optical microscopy (POM), differential scanning calorimetry (DSC), pressure-volume-temperature measurements (PVT), and wide-angle x-ray scattering (WAXS). POM and WAXS identified a liquid crystalline order up to high temperatures, whereas DSC and PVT, in addition, identified a glass transition. For the dynamics we have employed temperature- and pressure-dependent dielectric spectroscopy (DS). The aim is to (i) identify the relaxation mechanisms in the absence of solvent, (ii) obtain the most important parameters leading to glass formation, (iii) construct the relevant phase diagram (P-T), and finally, (iv) access the stability of phases under high pressures for these promising materials.

II. EXPERIMENT

Materials and structure. The polymer (PPP) consists of a poly(*p*-phenylene) backbone with sulfonate ester and dodecyl side groups and was synthesized by a Pd-catalyzed coupling of the 1,3-propanediol diester of 2-dodecyl-5-methyl-1,4-benzenediboronic acid with 2,2′-bis(3,5-di-*tert*-butylbenzenesulfonato)-4,4′-dibromobiphenyl. Details on the syn-

*Corresponding author. Email address: gfloudas@cc.uoi.gr

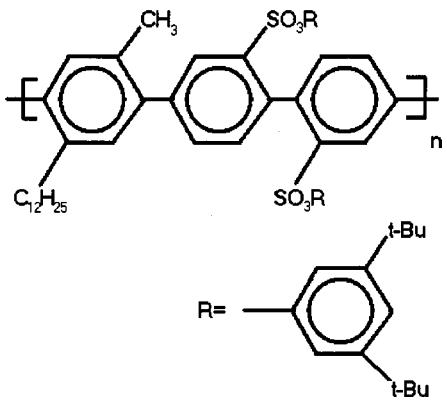

FIG. 1. Molecular structure of the poly(*p*-phenylenes) with the sulfonate ester and dodecyl side chains.

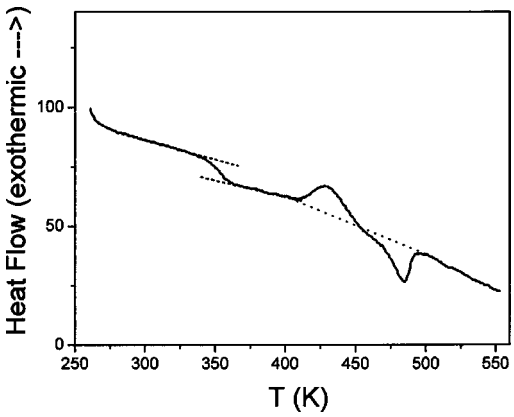

FIG. 2. DSC trace of P2 obtained on heating, indicating a glass transition at 357 K, followed by an exothermic peak at 430 K (structure reorganization) and by an endothermic peak at 485 K (structure melting).

thesis and characterization of the polymers, can be found elsewhere in detail [2]. Figure 1 gives the chemical structure of the samples and Table I their molecular characteristics.

Differential scanning calorimetry (DSC). A Mettler Toledo Star DSC capable of programmed cyclic temperature runs over the range 113–673 K was used. The samples were first heated with a rate of 10 K/min from ambient temperature to 550 K and then cooled to 250 K with the same rate. The second heating run (with the same rate), shown in Fig. 2 for P2, was used to identify a glass temperature at 357 K with an associated change in specific heat $\Delta c_p = 0.22$ J/gK, an exothermic peak at about 430 K with an associated heat of 6.8 J/g, and an endothermic peak at 485 K with a heat of fusion of about 5 J/g. These results will be discussed in connection with the results from the PVT and DS studies.

X-ray scattering. Wide-angle measurements were made with a Siemens θ-θ diffractometer (model D500T) in the reflection geometry. The Cu $K\alpha$ radiation was used from a Siemens generator (Kristalloflex 710 H) operating at 35 kV and 30 mA, and a graphite monochromator was utilized in front of the detector ($\lambda = 0.154$ nm). Measurements were made in the 2θ range from 0.1 to 40° in steps of 0.01° within the temperature range from 303 to 503 K. In addition, an oriented fiber of P8 was prepared using a miniextruder at 453 K and was subsequently investigated using a WAXS setup with a two-dimensional detector. The scattering from the fiber at 303 K is shown in Fig. 3.

Pressure-volume-temperature measurements. Pressure-volume-temperature (PVT) measurements were made using a fully automated GNOMIX high-pressure dilatometer. The PVT measurements were made on the P8 sample with $M_w = 4.4 \times 10^4$ g/mol. About 1 g was used in the measurements. First, we performed runs by changing pressures from 10 to 200 MPa (1 MPa=0.01 kbar) in steps of 10 MPa at constant temperatures (i.e., under ''isothermal'' conditions) from 293 to 510 K. Subsequently, measurements were made by heating/cooling experiments with a rate of 1 K/min at different fixed pressures (i.e., under ''isobaric'' conditions) in the range from 10 to 200 MPa. The 0.1 MPa data were obtained by extrapolation from the higher pressures.

TABLE I. Molecular characteristics of the $PPPSO_3$ samples.

Sample	M_w (Kg/mol)	M_w/M_n
P2	153	2.2
P4	104	2.1
P8	44	2.0

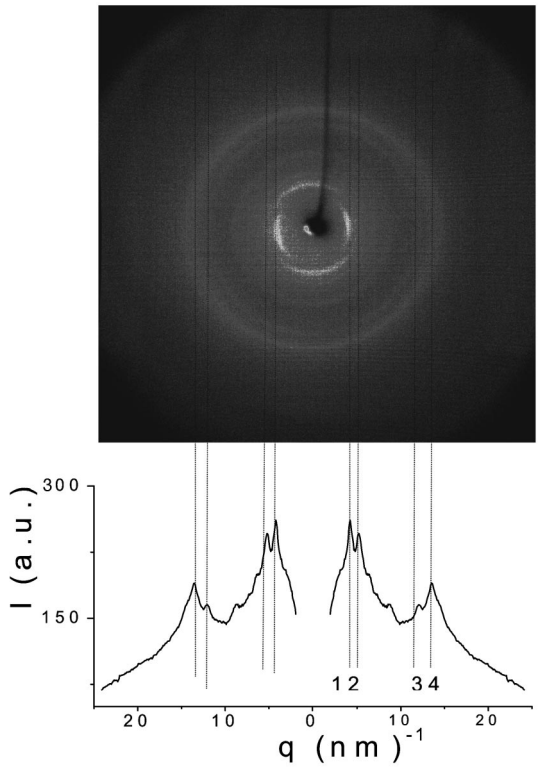

FIG. 3. (Top) WAXS profile from an oriented P2 fiber using a two-dimensional detector. Fiber orientation is along the vertical direction. (Bottom) Radially integrated intensity of the WAXS profile as a function of the wave vector. The vertical lines indicate the positions of the most intense reflections. Reflections are numbered consecutively (1, strong equatorial reflection; 2, strong meridional reflection).

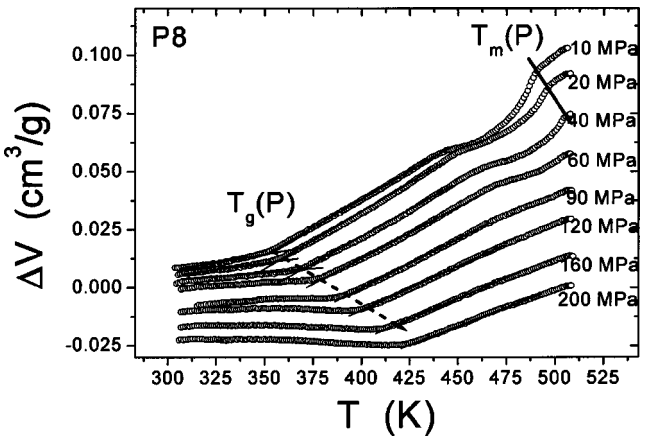

FIG. 4. Pressure-volume-temperature (PVT) measurements of P8 measured for pressures in the range from 10 to 200 MPa. The PVT measurements reveal a glass transition temperature followed by a melting temperature that are increasing functions of pressure. The dashed and solid lines give the approximate pressure dependence of the glass temperature (T_g) and of the melting temperature (T_m).

The result from the isobaric measurements is shown in Fig. 4 for the different pressures as indicated.

In the figure it is the relative change of specific volume (ΔV) that is plotted. A glass transition at 355 K and a melting temperature at 490 K are indicated by the change in slope and a discontinuous increase of ΔV, respectively. Notice that the effect of pressure (arrows in Fig. 4) is to increase both transition temperatures. These pressure effects will be compared with the corresponding effects in the dynamic investigation using dielectric spectroscopy.

Dielectric spectroscopy. The sample cell consisted of two electrodes with 20 mm in diameter and the sample with a thickness of 50 μm. The dielectric measurements were made at different temperatures in the range 123 to 453 K, for pressures in the range from 1 bar to 3 kbars (1 kbar $=100$ MPa), and for frequencies in the range from 10^{-2} to 3×10^{6} Hz using a Novocontrol BDS system composed from a frequency response analyzer (Solartron Schlumberger FRA 1260) and a broadband dielectric converter. The complex dielectric permittivity $\varepsilon^*=\varepsilon'$-$i\varepsilon''$, where ε' is the real and ε'' is the imaginary part, is a function of frequency ω, temperature T, and pressure P, $\varepsilon^*=\varepsilon^*(\omega,T,P)$. The setup for the pressure-dependent dielectric measurements consisted of the following parts: temperature controlled sample cell, hydraulic closing press with pump, and pump for hydrostatic test pressure. Silicon oil was used as the pressure transducing medium. In the pressure-dependent measurements the sample capacitor was sealed and placed inside a Teflon ring to separate the sample from the silicon oil.

In Fig. 5 some representative dielectric permittivity and loss spectra are shown for P2 at low and high temperatures. The spectra shown at low temperatures reveal a weak process in the glassy state (β process) whereas the spectra at higher temperatures show two processes beyond the process due to the ionic conductivity (i.e., the steep rise of the dielectric loss at low frequencies) and a process due to surface polarization indicated by the rise in the dielectric permittivity

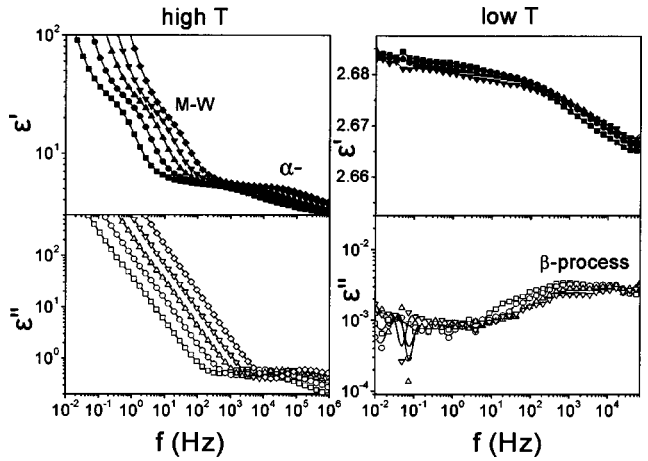

FIG. 5. Dielectric permittivity (ε') (top) and loss (ε'') (bottom) spectra of P2 shown at low and higher temperatures. The low T spectra indicate a weak β process in the glassy state. The high T spectra reveal two mechanisms associated with the glass transition and the Maxwell-Wagner polarization mechanisms.

values at lower frequencies. The two processes reflect the α process associated with the glass transition dynamics and the slower process due to the Maxwell-Wagner polarization mechanism (see below).

In the analysis of the DS spectra we have used the empirical equation of Havriliak and Negami (HN) [5,6]:

$$\frac{\varepsilon^*(T,P,\omega)-\varepsilon_\infty(T,P)}{\Delta\varepsilon(T,P)}=\frac{1}{\{1+[i\omega\tau_{\mathrm{HN}}(T,P)]^{\alpha}\}^{\gamma}}, \quad (1)$$

where $\tau_{\mathrm{HN}}(T,P)$ is the characteristic relaxation time in this equation, $\Delta\varepsilon(T,P)=\varepsilon_o(T,P)-\varepsilon\infty(T,P)$ is the relaxation strength of the process under investigation, and α, γ describe, respectively, the symmetrical and asymmetrical broadening of the distribution of relaxation times. In the fitting procedure we have used the ε'' values at every temperature and pressure and in some cases the ε' data were also used as a consistency check. The linear rise of the ε'' at lower frequencies is caused by the conductivity [$\varepsilon''\sim(\sigma_o/\varepsilon_f)\omega^{-1}$, where σ_o is the dc conductivity and ε_f is the permittivity of free space] which has been included in the fitting procedure.

III. RESULTS AND DISCUSSION

The DSC curve of P2 shown in Fig. 2 displays a glass temperature (at 357 K) followed by an exothermic peak (at about 430 K) associated with structure reorganization and by an endothermic peak (at 485 K) associated with the disappearance of the liquid crystalline order. The latter is confirmed by polarizing optical microscopy exhibiting birefringence up to this temperature. The liquid crystalline order originates from the packing and order along the backbone. Furthermore, the random position of the $C_{12}H_{25}$ groups along the chain is responsible for the absence of crystallization. The complete structural assignment can be made from the macroscopically oriented fiber using the two dimensional WAXS pattern of Fig. 3. The pattern displays strong equato-

rial and meridional reflections together with other more isotropic reflections at higher wave vectors. The radial integrated intensity is shown in the same figure and the peaks are identified with numbers. The primary equatorial reflection (depicted as 1) with a corresponding distance of about 1.6 nm is assigned to the interchain distance. The primary meridional reflection (2) with a corresponding distance of about 1.2 nm is assigned to intrachain correlations of the sulfonate ester group, i.e., to monomer size correlations. The two reflections at higher wave vectors (3 and 4) reflect the packing of the dodecyl side chains. Subsequently, the T dependence was investigated. The characteristic spacing corresponding to the primary equatorial reflection had a strong temperature dependence (not shown here). Since this reflection arises from interchain correlations the slope of the $d(T)$ dependence (between T_g and T_m the slope is 3.8×10^{-4} K^{-1}) reflects the coefficient of thermal expansion.

These structural findings are supported by the thermodynamic study using PVT (Fig. 4). Two transitions can be identified in the specific volume data at least for some low pressures. The change in slope in the relative specific volume, $\Delta V(T)$, at 10 MPa at about 355 K is in agreement with the DSC T_g. At higher temperatures the melting of the liquid crystalline structure can also be identified at about 490 K which again agrees with the DSC result. Notice that at about 440 K, the $\Delta V(T)$ has a peculiar dependence, suggesting structural reorganization on heating similar to what was found in DSC.

The results from the structure investigation (POM, DSC, WAXS, PVT) identified a liquid crystalline order composed from the rigid PPP backbones, up to 485 K. In addition, a glassy state exists below 357 K and structure reorganization takes place at about 430 K. Next we explore how these structural findings affect the dynamics as well as the effect of pressure on inducing orientational order.

The dynamics were investigated subsequently with dielectric spectroscopy and revealed three processes in all PPP's apart from the ionic conductivity at higher temperatures and/or low frequencies. Starting from lower temperatures, the dielectric permittivity and loss spectra (Fig. 5) reveal a broad ($\alpha=0.33\pm0.03$, $\gamma=1$) localized dipolar relaxation, called the β process. The strength of the process ($T\Delta\varepsilon \sim 2$ K) and its Arrhenius temperature dependence (Fig. 6)

$$\log \tau = \log \tau_0^* + \frac{E}{2.303RT}, \tag{2}$$

where τ_0^* is the characteristic time at very high temperatures and E is the apparent activation energy (Table II), are suggestive of a partial dipolar relaxation of the side chain comprising the sulfonate ester group. We mention here, parenthetically, that a β process was found in poly(p-phenylenes) with short ethylene oxide (EO) side chains [3] with an activation energy of 8 kcal/mol, which, based on NMR was identified as being due to the outer EO units. The results for the apparent activation energy (Table II) reveal some dependence on the chain length that is not the norm for a localized motion well below T_g. As for the molecular assignment, preliminary NMR studies as a function of temperature identified the sulfonate ester side chain as well as the substituted ring with the dodecyl chains as responsible for the β process. Therefore, both the sidechain and the backbone contribute to this process.

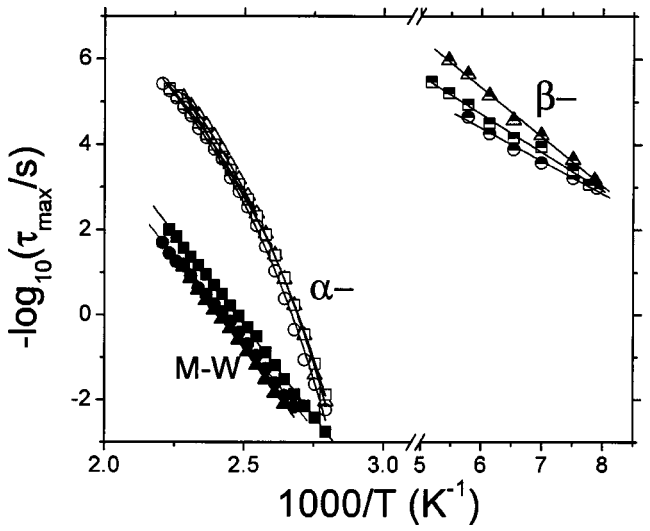

FIG. 6. Relaxation map of the different processes in P2 (circles), P4 (squares), and P8 (triangles) in the usual Arrhenius representation. Three processes are shown associated with the β process (half-filled symbols), the segmental α process (open symbols) and a "slow" process due to the Maxwell-Wagner polarization (filled symbols). Lines are fits to the Arrhenius (β process and Maxwell-Wagner mechanism) and VFT (α process) equations.

At higher temperatures, the response is dominated by the α process ($T\Delta\varepsilon \sim 900$ K) displaying a strong T dependence that can be described by the Vogel-Fulcher-Tammann (VFT) equation:

$$\log \tau_{\max} = \log \tau_0 + \frac{DT_0}{T-T_0}, \tag{3}$$

where τ_0 is the limiting value at high temperatures, B ($=DT_0$) is the apparent activation energy, and T_0 the "ideal" glass temperature. The parameters $\log \tau_0$, D, and T_0 are summarized in Table II. Notice that the α-relaxation times are nearly indistinguishable for the three samples, implying that they all freeze at the same T_g and have the same apparent activation energy. The molecular origin of the α process cannot be easily identified in the present system as opposed to the PPP system with the short EO side chains because the present structure in not as favorable for NMR. Nevertheless, NMR studies on the present system identified unfreezing of the backbone at temperatures above 350 K, i.e., a similar situation as with the PPP(EO) system [3].

A slower, very intense process (i.e., $T\Delta\varepsilon \sim 9000$ in P2) with an Arrhenius T dependence and a Debye-like distribution (see below) was found in all samples. This process is identified as due to Maxwell-Wagner polarization [6] originating from the presence of a residual Pd catalyst (aggregates of size 2–5 nm). Despite their low concentration (0.1% to 0.2%) these aggregates create a heterogeneous dielectric environment. The shape parameters and their temperature de-

TABLE II. Activation parameters for the different relaxation processes in P2, P4, and P8.

	Polymer P2			Polymer P4			Polymer P8		
	α	β	MW	α	β	MW	α	β	MW
$-\log(\tau_0/s)$	12.2	9.0	20	11.85	10.1	21.2	12.4	12.2	21.3
E (kcal/mol)		3.5	38		4.08	39.3		5.27	40.3
D	4.13			3.94			4.11		
T_0 (K)	279			279			279		

pendence for the two processes is shown in Fig. 7. Notice that the distribution, for the α process, is not symmetric and, moreover, there is a spectral narrowing above 430 K, i.e., within the temperature range where structure reorganization takes place. The latter implies that structure reorganization is assisted by segmental motions. Overall, within the broad temperature range investigated, the α process does not obey the principle of time-temperature-superposition (tTs), i.e., the system is thermorheologically complex at the segmental level. The origin of the broadening of the α process is largely intramolecular as shown by the solution study [4].

Next we discuss the phase behavior of PPP's. For this purpose we employ a pressure-dependent dielectric investigation in conjunction with the PVT results. The effect of pressure was investigated mainly on the α process and the slower process due to Maxwell-Wagner (MW) polarization. The effect of pressure on the dielectric loss spectra of P2 is shown in Fig. 8 at 433 K.

Both the α and the process due to the MW polarization become slower with increasing pressure. The analysis of the relaxation times, however, shows that the MW process is only moderately affected by pressure in contrast to the strong slow down of the α process. The relaxation times at maximum loss for the two processes are plotted in Fig. 9 and display a linear pressure dependence within the investigated pressure range.

The linear dependence of $\log\tau$ with P can be used to define an apparent activation volume ΔV as [7]

$$\Delta V = 2.303RT\left(\frac{\partial \log \tau}{\partial P}\right)_T \tag{4}$$

and its T dependence is plotted in the inset to Fig. 9. Notice the strong T dependence of this quantity for the α process as found in other polymers and glass-forming liquids [8]. Contrast this with the nearly T-independent apparent activation volume for the slower process which lacks a molecular origin. Notice that the apparent activation volume for the α process is much smaller than the volume required for a monomer unit to rotate about its backbone (a broad estimate gives 2800 cm^3/g), suggesting localized motions as the origin of the process within the temperature range T_g+60 to T_g+100 K.

One central issue in liquid-to-glass dynamics is defining the controlling parameter leading to glass formation [9–12]. In free volume theories, volume is the only controlling parameter and a glass is formed as a result of insufficient free

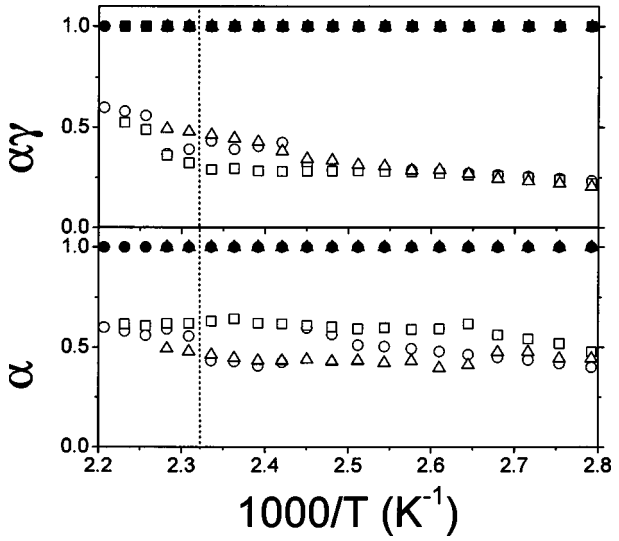

FIG. 7. Temperature dependence of the HN shape parameters (α and $\alpha\gamma$) for the α process (open symbols) and the slower process due to the Maxwell-Wagner polarization (filled symbols) for the three samples: P2 (circles), P4 (squares), and P8 (triangles). The vertical line indicates the onset of structure reorganization (T = 430 K from DSC).

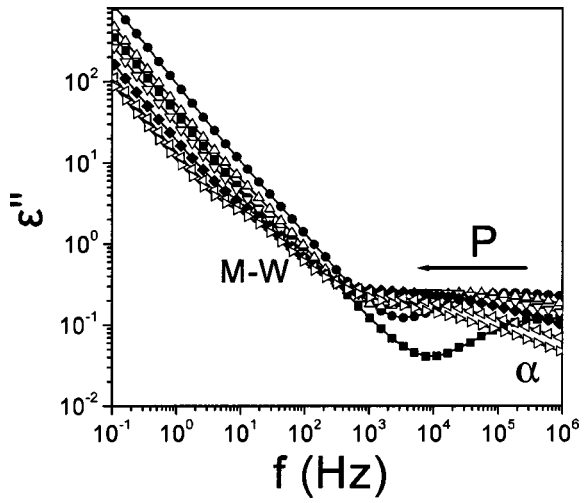

FIG. 8. Dielectric permittivity (ε') and loss (ε'') spectra of P2 at 433 K for different pressures: ■, P = 0.1 MPa; ●, P = 30 MPa; △, P = 60 MPa; ▽, P = 90 MPa; ◆, P = 120 MPa; ◁, P = 150 MPa; ▷, P = 180 MPa. The two relaxation mechanisms (the α process and the process due to the Maxwell-Wagner polarization mechanism) are shown.

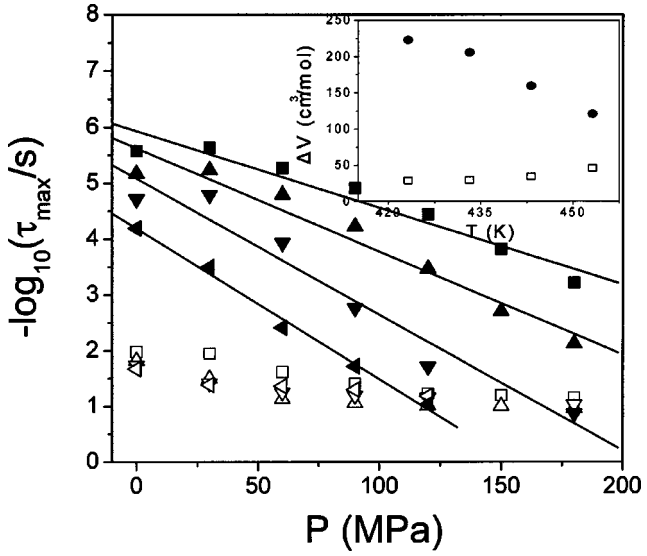

FIG. 9. Pressure dependence of the relaxation times at maximum loss for the polymer P2, corresponding to the α process (filled symbols) and the slower process due to the Maxwell-Wagner polarization (open symbols) at four different temperatures: ■, $T=453$ K; ▲, $T=443$ K; ▼, $T=433$ K; and ◀, $T=423$ K. In the inset, the apparent activation volume of the α (filled symbols) and of the Maxwell-Wagner (open symbols) processes is plotted as a function of temperature. Notice that the α process possesess the highest apparent activation volume with the stronger temperature dependence.

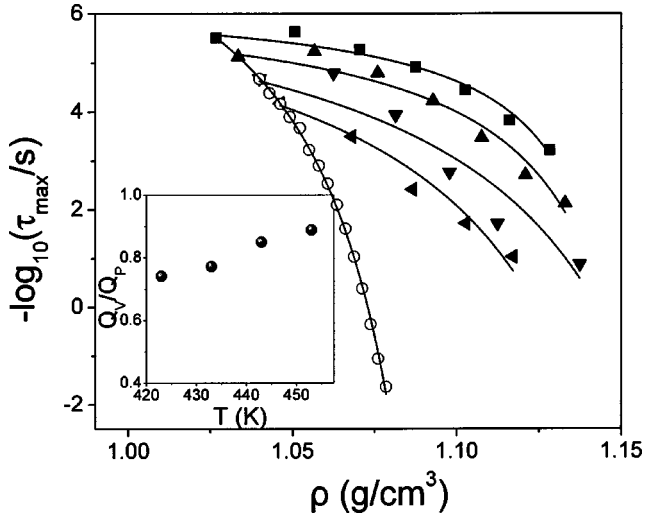

FIG. 10. Relaxation times (the α process) plotted as a function of density: open symbols, obtained by changing temperature under ''isobaric'' conditions at $P=0.1$ MPa; filled symbols, obtained by changing pressure under ''isothermal'' conditions. ■, $T=453$ K; ▲, $T=443$ K; ▼, $T=433$ K; and ◀, $T=423$ K. In the inset, the ratio of apparent activation energies under constant volume and constant pressure is given (calculated at $P=0.1$ MPa). Notice that the ratio assumes values well above 0.5, suggesting the dominance of thermal effects over volume in glass formation.

volume (normally when the free volume is only 2.5% of the total volume). If the process is purely activated then temperature is the controlling parameter; by lowering T there is insufficient thermal energy to cross an energy barrier required for the motion. Since changing temperature alone affects both the thermal energy and the volume, an additional parameter is required to decouple the two effects. This is possible through the application of pressure that can be applied under isothermal conditions, i.e., affecting solely the density (or volume) and not the temperature. Then the relaxation times under ''isothermal'' and ''isobaric'' conditions can be cast together on a single representation (using the PVT data) by plotting the relaxation times as a function of density in Fig. 10.

For a quantitative comparison the apparent activation energies at constant volume $[Q_V=-RT^2(\partial \ln \tau/\partial T)_V]$ and pressure $[Q_P=-RT^2(\partial \ln \tau/\partial T)_P]$ are needed. These quantities can be obtained from the $\tau(T)$ dependencies under isochoric and isobaric representations, respectively. Then a ratio of Q_V/Q_P near 0 would imply that volume is the dominant parameter whereas a value near 1 would suggest thermal energy as the controlling parameter. The ratio Q_V/Q_P calculated at atmospheric pressure is plotted in the inset to Fig. 10 and shows that glass formation is dominated by thermal energy rather than volume. The highly packed structures already in the melt state make the system less prone to volume variations. On the other hand, the freezing of backbone rotational freedom by lowering temperature seems to be the dominant parameter in rigid rod polymers, resulting in glass formation. This finding is in agreement with the intramolecular character of the α process suggested by the dilute solution studies of the same material [4]. We mention here that thermal energy was also the dominant parameter governing glass formation in polypeptides [13] and polyalcohols [12,14], i.e., in systems with strong hydrogen bonds. This situation for the hairy-rod polymers studied here, as well as for the hydrogen bonded systems mentioned above, is in contrast to the situation found in flexible polymers and glass-forming liquids [9–12], where volume is equally important to thermal energy.

The results of the PVT and the pressure-dependent dielectric investigation can be combined in a single phase diagram (T-P) [10,15,16]. This is shown in Fig. 11 depicting the $T_g(P)$ and $T_m(P)$ dependencies for P8. We mention here that this should be considered as a ''pseudo'' phase diagram in the sense that not all phases are at equilibrium (i.e., the glassy ''phase''). Furthermore, despite the phase coexistence in lines, there is no triple point (the latter would require negative pressures). In DS, the T_g is operationally defined as a temperature corresponding to a relaxation time of 10^2 s. In PVT, the $T_g(P)$ is already defined by the change in the specific volume in Fig. 4. The two independent definitions of T_g, one dynamic and the other purely thermodynamic, are in excellent agreement. Both can be described by the empirical equation [17]:

$$T_g(P)=T_g(0)\left(1+\frac{b}{a}P\right)^{1/b} \tag{5}$$

where $T_g(0)$ is the glass temperature at atmospheric pressure

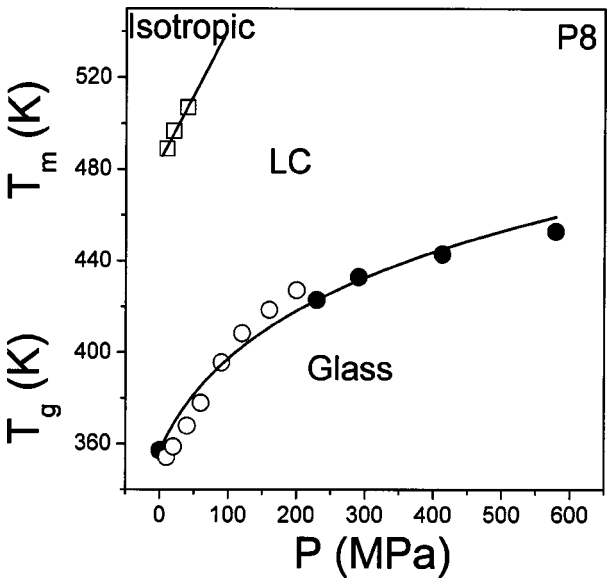

FIG. 11. Phase diagram of P8 displaying an isotropic phase at high temperatures, a liquid crystalline state, and a glass phase at lower temperatures. The pressure dependence of the smectic-to-isotropic transition (open squares) is used to extract the change of volume associated with this first-order transition. For the glass transition, both the DS data (filled circles) and the PVT data (open circles) are used. In DS the T_g is operationally defined as the temperature corresponding to a relaxation time of 100 s.

and a, b are fitting parameters. The use of the above equation to the combined results for the $T_g(P)$ results in $a=5.3$ MPa and $b=9.7$.

In the same T-P representation the $T_m(P)$ dependence, obtained from PVT, is also shown. Notice that $T_m(P)$ has a linear pressure dependence (as expected for a true first-order transition), in contrast to the $T_g(P)$. The slope dP/dT of $T_m(P)$ can be used to calculate the change in specific volume (ΔV) at the transition from the Clausius-Clapeyron equation [18]:

$$\frac{dP}{dT}=\frac{\Delta H}{T\Delta V}, \tag{6}$$

where $T=485$ K, $dP/dT=1.7$ MPa/K from Fig. 11, and $\Delta H=5$ J/g from DSC. The resulting ΔV, of 6×10^{-3} cm^3/g, is in good agreement with the change in specific volume found in the PVT measurements (Fig. 4).

There are some implications from the phase diagram shown—because of the different T_m and T_g pressure dependencies, increasing pressure results in a larger region in the phase diagram where the liquid crystalline phase is stable, i.e., pressure effectively stabilizes the liquid crystalline mesophase. Moreover, the liquid crystalline phase formed at elevated pressures near the borders to the isotropic state is more mobile [a greater $\Delta T(P)=T_m(P)$-$T_g(P)$ difference] as compared to the same phase formed at atmospheric pressure. These results suggest a large effect of pressure not only on the *mobility* but also on the *stability* of the liquid crystalline mesophase that could find some applications in fuel cell technology.

IV. CONCLUSIONS

The investigation of the structure and mobility in a system of high orientational order comprising poly(p-phenylenes) with sulfonate ester and dodecyl side chains in the absence of solvent revealed the following.

(1) Rigid rod poly(p-phenylenes) with sulfonate ester and dodecyl side chains form highly anisotropic structures with liquid crystalline order up to 485 K at atmospheric pressure (WAXS, POM, DSC, PVT).

(2) Three dynamic processes exist associated with (i) localized dipolar relaxations of the sulfonate ester side chain as well as of the substituted ring with the dodecyl chains in the glassy state (β process), (ii) an α process associated with the glass transition, and (iii) a slower process of higher intensity associated with the Maxwell-Wagner polarization associated with the presence of small amounts of palladium catalyst. It is surprising that such systems with high orientational order show an α process—which is thought to exist only in amorphous polymers and glass-forming liquids—but the origin of this process associates with the unfreezing of the backbone dynamics. From the ratio of activation energies at constant volume and pressure we conclude that the main control parameter giving rise to glass formation in rigid rod polymers is temperature rather than volume (i.e., $Q_V/Q_P>0.5$).

(3) Pressure was found to induce the liquid crystal–to–isotropic transition following basic thermodynamics (the Clausius-Clapeyron equation for first order transitions) and the calculated change of volume is in agreement with the measured change of volume from PVT. Pressure induces also the glass transition but to a lesser extent. The $T_g(P)$ dependence as obtained from a dynamic study (DS) is in very good agreement with the same dependence obtained from the ''static'' investigation (PVT). Based on the constructed phase diagram, we find that the different pressure dependencies of T_m and T_g result in a more stable (over a broader T range), albeit more mobile, liquid crystalline mesophase, at elevated pressures.

ACKNOWLEDGMENTS

We thank Dr. R. Graf (MPI-P) for stimulating discussions on NMR as well as for the NMR experiments, A. Best (MPI-P) for the PVT measurements, and G. Tsoumanis for technical support at the University of Ioannina.

[1] G. Wegner, Macromol. Chem. Phys. **204**, 347 (2003).
[2] S. Vanhee, R. Rulkens, U. Lehmann, C. Rosenauer, M. Schulze, W. Köhler, and G. Wegner, Macromolecules **29**, 5136 (1996).
[3] M. Mierzwa, G. Floudas, M. Neidhöfer, R. Graf, H.W. Spiess, W.H. Meyer, and G. Wegner, J. Chem. Phys. **117**, 6289 (2002).
[4] M. Bockstaller, G. Fytas, and G. Wegner, Macromolecules **34**, 3497 (2001).

[5] S. Havriliak and S. Negami, Polymer **8**, 161 (1967).
[6] N.G. McCrum, B.E. Read, and G. Williams, in *Anelastic and Dielectric Effects in Polymeric Solids* (Dover, New York, 1991).
[7] G. Floudas, in *Broadband Dielectric Spectroscopy*, edited by F. Kremer and A. Schönhals (Springer, Berlin, 2002), Chap. 8.
[8] G. Floudas, C. Gravalides, T. Reisinger, and G. Wegner, J. Chem. Phys. **111**, 9847 (1999).
[9] G. Williams, Trans. Faraday Soc. **60**, 1548 (1964); **60**, 1556 (1964).
[10] K. Mpoukouvalas and G. Floudas, Phys. Rev. E **68**, 031801 (2003).
[11] M. Paluch, R. Casalini, A. Patkowski, T. Pakula, and C.M. Roland, Phys. Rev. E **68**, 031802 (2003).
[12] M.L. Ferrer, C. Lawrence, B.G. Demirjian, D. Kivelson, C. Alba-Simionesco, and G. Tarjus, J. Chem. Phys. **109**, 8010 (1998).
[13] P. Papadopoulos, G. Floudas, H.-A. Klok (unpublished).
[14] S. Hensel-Bielowka, M. Paluch, and C.M. Roland, J. Phys. Chem. B **106**, 12459 (2002).
[15] M. Mierzwa, G. Floudas, and A. Wewerka, Phys. Rev. E **64**, 031703 (2001).
[16] G. Floudas, M. Mierzwa, and A. Schönhals, Phys. Rev. E **67**, 031705 (2003).
[17] S.P. Andersson and O. Andersson, Macromolecules **31**, 2999 (1998).
[18] M. Mierzwa, G. Floudas, P. Stepanek, and G. Wegner, Phys. Rev. B **62**, 14012 (2000).